Hindawi
Complexity
Volume 2019, Article ID 8271584, 13 pages
https://doi.org/10.1155/2019/8271584

Research Article

Implementation of a Controller to Eliminate the Limit Cycle in the Inverted Pendulum on a Cart

Mayra Antonio-Cruz,[1,2] **Victor Manuel Hernández-Guzmán**,[3] **Ramón Silva-Ortigoza**,[1] **and Gilberto Silva-Ortigoza**[4]

[1] *Instituto Politécnico Nacional, CIDETEC, Área de Mecatrónica y Energía Renovable, 07700 Mexico City, Mexico*
[2] *Instituto Politécnico Nacional, UPIICSA, SEPI, 08400 Mexico City, Mexico*
[3] *Universidad Autónoma de Querétaro, Facultad de Ingeniería, 76010 Querétaro, QRO, Mexico*
[4] *Benemérita Universidad Autónoma de Puebla, Facultad de Ciencias Físico Matemáticas, 72570 Puebla, PUE, Mexico*

Correspondence should be addressed to Victor Manuel Hernández-Guzmán; vmhg@uaq.mx

Received 28 July 2018; Revised 14 November 2018; Accepted 27 November 2018; Published 4 February 2019

Guest Editor: Carlos-Arturo Loredo-Villalobos

A frequency response-based linear controller is implemented to regulate the inverted pendulum on a cart at the inverted position. The objective is to improve the performance of the control system by eliminating the limit cycle generated by the dead-zone, induced by static friction, at the actuator of the mechanism. This control strategy has been recently introduced and applied by the authors to eliminate the limit cycle in the Furuta pendulum and the pendubot systems. Hence, the main aim of the present paper is to study the applicability of the control strategy to eliminate the limit cycle in the inverted pendulum on a cart. The successful results that are obtained in experiments corroborate that the approach introduced by the authors to eliminate the limit cycle in the Furuta pendulum and pendubot is also valid for the inverted pendulum on a cart.

1. Introduction

Friction is a phenomenon that can cause nonlinear behavior in mechanical systems involving motion [1]. Such a nonlinear behavior refers, in particular, to a dead-zone [2] which degrades performance of the overall system by generating position error, limit cycle, and even instability [3]. These problems, separately, have been important subjects of study. As a matter of fact, compensation of friction in mechanical systems has been carried out to achieve a better control of position [4–8]. Limit cycles generated by the static and Coulomb friction have been treated in [1, 9–14] and the stability analysis of systems with friction has been introduced in [15–17]. On the other hand, underactuated mechanical systems, and in particular inverted pendulums, have attracted the attention of several researchers because they are an excellent benchmark to study position control, limit cycles, and system stability [18]. Motivated by this scenario and by [19, 20], this paper deals with the elimination of limit cycles generated by a friction-induced dead-zone nonlinearity when regulating the inverted pendulum on a cart.

Different authors have reported important results on limit cycles in the regulation of inverted pendulums which, in general, can be divided into three categories: *(a) generation of stable limit cycles*, *(b) reduction of limit cycles*, and *(c) elimination of limit cycles*.

Regarding *(a)*, Verduzco [21] presented a method for nonlinear systems that have k zero eigenvalues when they are linearized. Such a method contemplates the existence of a curve of Hopf bifurcation points and a change of both coordinates and input control. The pendubot was used to illustrate the method. Also, for the pendubot, Freidovich et al. [22] proposed a feedback control strategy based on motion planning via virtual holonomic constraints. Furthermore, Freidovich et al. [23] developed a control for the Furuta pendulum, which was integrated by a shaping energy control, a passivity-based control, and an auxiliary feedback action.

Andary et al. [24] introduced a control based on partial nonlinear feedback linearization and dynamic control. Aguilar et al. [25] used partial feedback linearization with a two-relay controller, which was tuned with the classic tool root locus. The two latter works are for the inertia wheel pendulum.

For *(b)*, Medrano-Cerda [26] considered a scheme based on velocity-sign compensation in the inverted pendulum on a cart. Also, Vasudevan et al. [27] compensated friction via a passivity-based observer for the wheeled inverted pendulum. Eom and Chwa [28] compensated friction, system uncertainties, and an external disturbance through a nonlinear observer for the pendubot.

With regard to *(c)*, Hernández-Guzmán et al. [19] exploited the differential flatness property of the Furuta pendulum to propose a linear state feedback controller which can be designed to regulate the system and to eliminate limit cycles. To achieve this, an educational, experimental, and intuitive procedure based on the time response approach, i.e., root locus, was introduced. As an improvement, Antonio-Cruz et al. [20] presented a modified version of the control in [19]. The design of such a modified control was based on frequency response, instead of time response as in [19], which entailed the obtention of precise formulas that facilitates the limit cycle elimination. A comparison of [19, 20] showed that [20] has better performance when dealing with the limit cycle elimination. On the other hand, some studies that consider the backlash nonlinearity in the Furuta pendulum and cart-pendulum system [29, 30] have been reported. Other papers dealing with performance improvement of inverted pendulums have been reported [31–34]. Finally, papers related to dead-zone compensation for nonlinear systems and suppression of limit cycles in servomechanism are [35–39].

Having undertaken the literature review, it was found that the papers dealing with reduction of friction-induced limit cycles use compensation techniques that have the following disadvantages: (i) most compensation terms are complex and require the numerical values of the frictional parameters [27] and (ii) undercompensation leads to steady-state error and overcompensation may induce limit cycles [9, 40]. Although an important effort has been done in [26] to reduce the limit cycle in the inverted pendulum on a cart, to the authors' knowledge, the elimination of the limit cycle in the inverted pendulum on a cart has not been achieved until now. On the other hand, only two previous papers [19, 20] have achieved limit cycle elimination without using compensation techniques but just by employing a simple linear controller. In both papers the controller was proposed by using a differential flatness representation of the system and the describing function method was employed to study the existence of limit cycles. In [19] the controller was designed via the time response approach (root locus) and in [20] via the frequency response approach (Bode diagrams). Since the root locus is not intrinsically related to the describing function method, the corresponding design procedure presented in [19] is based on intuitive ideas because precise formulas were not obtained. According to [20], this renders the repetition of the result when using a different Furuta pendulum difficult. Hence, [20] presented a simple and precise procedure to eliminate limit cycles caused by the friction-induced dead-zone nonlinearity. In that direction, the controller and the design procedure for limit cycle elimination introduced in [20], for the Furuta pendulum and pendubot systems, are applied to the inverted pendulum on a cart in the present paper with the aim of investigating the possibility to eliminate the limit cycle in this underactuated mechanism.

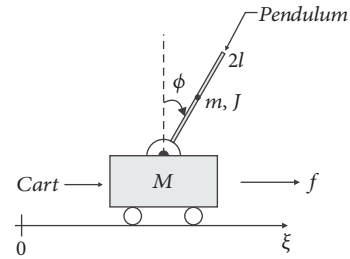

Figure 1: Inverted pendulum on a cart.

It is recalled that the advantage of the controller proposed in [20] with regard to compensation techniques is that the model or the characterization of the dead-zone is not required, whereas the advantage with regard to [19] is that the combination of the describing function method and frequency response allows providing precise formulas that render the design of the linear controller and, in consequence, the experimental elimination of limit cycles easier.

The rest of the paper is organized as follows. Section 2 presents the differential flatness model of the linear approximation of the inverted pendulum on a cart, as well as a description of the real prototype used in experiments. Section 3 presents the linear controller to regulate the inverted pendulum on a cart and the procedure to design it. The procedure to eliminate the dead-zone nonlinearity-induced limit cycles in the system is briefly described in Section 4. Lastly, Section 5 gives the conclusions.

2. Inverted Pendulum on a Cart

This section presents the differential flatness model of the inverted pendulum on a cart, as well as the description of the prototype used in the experimental procedure to eliminate limit cycle.

2.1. Flatness Model. The inverted pendulum on a cart shown in Figure 1 consists of a cart that has linear motion on a limited rail, in the horizontal plane, and in one dimension. This motion is due to a force applied by a transmission system actuated by a motor. On the cart, a pendulum is attached which can move angularly in the vertical plane which is parallel to the cart movement. The parameters and variables of this system appear in Figure 1 and are denoted as follows. M and ξ are the mass and the translational position of the cart, respectively, whereas m, $2l$, and ϕ are the mass, length, and angular position of the pendulum, respectively. Lastly, f is the force applied to the cart and g is acceleration of gravity.

The approximate linear model of the inverted pendulum on a cart,

$$\dot{x}_\delta = \mathscr{A} x_\delta + \mathscr{B} u_\delta \tag{1}$$

with

$$x_\delta = \begin{bmatrix} x_{\delta 1} \\ x_{\delta 2} \\ x_{\delta 3} \\ x_{\delta 4} \end{bmatrix} = \begin{bmatrix} \xi - \overline{\xi} \\ \dot{\xi} - \overline{\dot{\xi}} \\ \phi - \overline{\phi} \\ \dot{\phi} - \overline{\dot{\phi}} \end{bmatrix}, \qquad u_\delta = f - \overline{f}, \tag{2}$$

$$\mathscr{A} = \begin{bmatrix} 0 & 1 & 0 & 0 \\ 0 & 0 & -\dfrac{mg}{M} & 0 \\ 0 & 0 & 0 & 1 \\ 0 & 0 & \dfrac{(M+m)\,g}{lM} & 0 \end{bmatrix}, \qquad \mathscr{B} = \begin{bmatrix} 0 \\ \dfrac{1}{M} \\ 0 \\ -\dfrac{1}{lM} \end{bmatrix}, \tag{3}$$

around the operation point

$$\begin{bmatrix} \overline{\xi} & \overline{\dot{\xi}} & \overline{\phi} & \overline{\dot{\phi}} \end{bmatrix}^T = \begin{bmatrix} 0 & 0 & 0 & 0 \end{bmatrix}^T, \qquad \overline{f} = 0, \tag{4}$$

is controllable [41] and, in consequence, is differentially flat [42], Ch. 2. Therefore, the flat output F, associated with (1), is defined by [42], Ch. 2:

$$F = \lambda \begin{bmatrix} 0 & 0 & 0 & 1 \end{bmatrix} C_0^{-1} x_\delta, \tag{5}$$

where λ is an arbitrary nonzero constant, conveniently chosen as $\lambda = -g/(lM)$, and $C_0 = \begin{bmatrix} \mathscr{B} & \mathscr{A}\mathscr{B} & \mathscr{A}^2\mathscr{B} & \mathscr{A}^3\mathscr{B} \end{bmatrix}$ is the controllability matrix of system (1). After calculations F and its first four time derivatives are obtained:

$$F = x_{\delta 1} + l x_{\delta 3}, \tag{6}$$

$$\dot{F} = x_{\delta 2} + l x_{\delta 4}, \tag{7}$$

$$\ddot{F} = g x_{\delta 3}, \tag{8}$$

$$F^{(3)} = g x_{\delta 4}, \tag{9}$$

$$F^{(4)} = \frac{(M+m)\,g}{lM} \ddot{F} - \frac{g}{lM} u_\delta. \tag{10}$$

This last expression represents the differential flat model that describes the dynamics (1) and since $\overline{f} = 0$, it can be written as

$$f = (M+m)\,\ddot{F} - \frac{lM}{g} F^{(4)}. \tag{11}$$

2.2. Description of the Prototype. The prototype of the inverted pendulum on a cart used in the experimental procedure to eliminate limit cycle is shown in Figure 2. In general, this prototype has four subsystems: (i) Mechanical structure, (ii) actuator and sensors, (iii) power stage, and (iv) data acquisition and processing, which are described below.

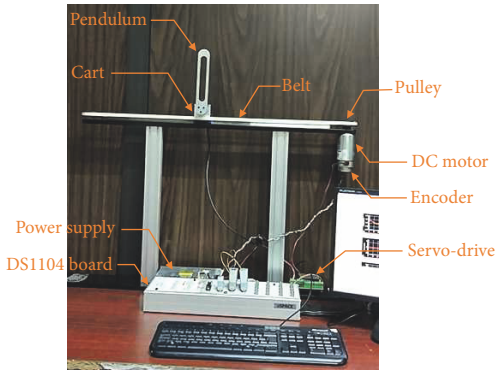

Figure 2: Prototype of the inverted pendulum on a cart.

(i) *Mechanical structure* refers to the mechanical elements that compose the mechanism, that is, a cart mounted on a limited rail, the transmission system (toothed belt and two pulleys), and the pendulum.

(ii) *Actuator and sensors* consist in a Pittman 14204S006 DC motor and two incremental encoders used to measure the angular positions of the pulleys and pendulum. Since the DC motor is connected to one pulley, the angular position of this pulley is used to compute the linear position of the cart. The encoder used to measure the angular position of the pulley has 500 PPR and is included in the chassis of the motor. The encoder used to measure the angular position of the pendulum has 1024 PPR and is fabricated by Baumer in the model ITD01B14.

(iii) *Power stage* is integrated by an HF100W-SF-24 switched power supply and an AZ12A8DDC servo-drive manufactured by Advanced Motion Controls. This latter possesses an inner current-loop driven by a PI controller, which ensures that the current of the DC motor, i_m, reaches the current imposed by the control signal, i, that is, $i_m \longrightarrow i$. This means that a desired torque signal can be implemented through the dynamic relation of torque-current: $\tau = k_m i \approx k_m i_m$, where τ and k_m are the torque and torque constant of the DC motor, respectively. Since the input of the inverted pendulum on a cart is the force f, the desired torque is converted to the desired force by using $\tau = fr$, with r being the radius of the pulley connected to the DC motor.

(iv) *Data acquisition and processing* corresponds to a DS1104 board from dSPACE, Matlab-Simulink, and ControlDesk. Through this hardware and software the variables of the system are read, which allows implementation of the controller. It is important to say that, in all experiments, the velocities $\dot{\xi}$ and $\dot{\phi}$ were estimated via a derivative block of Simulink and the sampling period was set to 1 ms.

The mechanical parameters of the inverted pendulum on a cart are presented below, which were found by measuring the length of the pendulum and weighing the cart and pendulum.

$2l = 0.200 \times 10^{-3}$ m,

$m = 0.034$ kg,

$M = 0.385$ kg.

3. Linear Controller

This section presents a linear state feedback controller for position regulation in the inverted pendulum on a cart, which is derived by considering flat model (11). Also, the analysis of the existence of limit cycles is given and the procedure to design the controller is described.

3.1. Controller Proposal. On the one hand, after applying the Laplace transform to (11), the following transfer function is obtained:

$$\frac{F(s)}{f(s)} = \frac{-g/(lM)}{s^2\left[s^2 - g(M+m)/(lM)\right]}, \tag{12}$$

where $F(s)$ and $f(s)$ stand for Laplace transforms of the flat output and the applied force, respectively.

On the other hand, the dead-zone nonlinearity has the characteristic function shown in Figure 3, whose parameters are described in [19]. An approximate frequency response description of a dead-zone nonlinearity is the following describing function [43], Ch. 5, where it is assumed that the nonlinearity input e is a sinusoidal function of time with amplitude A and frequency ω:

$$N(A) = \frac{2k}{\pi}\left[\frac{\pi}{2} - \arcsin\left(\frac{\delta}{A}\right) - \frac{\delta}{A}\sqrt{1-\left(\frac{\delta}{A}\right)^2}\right]. \tag{13}$$

This "transfer function," $N(A)$, is real, positive, and frequency independent but dependent on the input amplitude A. Its maximal value is $N(A) = k > 0$, which is reached as $A \longrightarrow \infty$, and its minimal value tends to zero if $A \longrightarrow \delta$.

Since transfer function (12) has similar characteristics to that of the Furuta pendulum obtained in [19, 20], hence, the control scheme proposed in [20] to control the Furuta pendulum and the pendubot, that is,

$$f(s) = k_v F(s) s^3 + \beta F(s) s^2 + k_d F(s) s + k_p F(s), \tag{14}$$

where k_v, β, k_d, and k_p are the control gains, is also used to control (12). The block diagram of the plant (12) in closed loop with controller (14) and considering the dead-zone nonlinearity is shown in Figure 4. There, positive feedback is used due to $-g/(lM) < 0$.

Lastly, when considering the linear state feedback controller

$$u_\delta = f = -k_1 x_{\delta 1} - k_2 x_{\delta 2} - k_3 x_{\delta 3} - k_4 x_{\delta 4}, \tag{15}$$

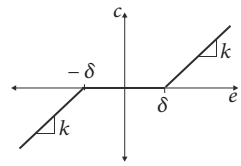

Figure 3: Representation of a dead-zone nonlinearity.

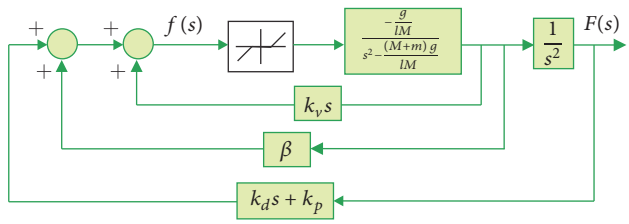

Figure 4: Closed-loop system considering a dead-zone nonlinearity.

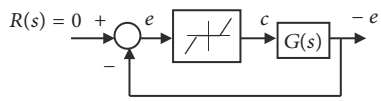

Figure 5: Equivalent representation of block diagram in Figure 4.

where k_1, k_2, k_3, and k_4 are the gains of the controller, u_δ and x_δ stand as defined previously in (2), and using (6)-(10), the following equivalence between (14) and (15) is found:

$$\begin{aligned} k_1 &= -k_p, \\ k_2 &= -k_d, \\ k_3 &= -\left(\beta g + l k_p\right), \\ k_4 &= -\left(k_v g + l k_d\right). \end{aligned} \tag{16}$$

3.2. Analysis of Limit Cycle Existence. The analysis of limit cycle existence in the inverted pendulum on a cart is carried out as in [19, 20] for the Furuta pendulum and pendubot, that is, by using the *describing function method*. This is because the approximation of the dead-zone nonlinearity is based on the describing function.

The describing function method [43], Ch. 5, suggests representing the system in the standard form shown in Figure 5. Also, such a method requires that the linear time invariant system $G(s)$ behaves as a low-pass filter. Thus, the standard form is obtained applying block algebra on Figure 4. In this case, the nonlinearity input is $e = f(s)$ while the linear time invariant system $G(s)$ is

$$G(s) = G_1(s) G_2(s), \tag{17}$$

where

$$G_1(s) = \frac{g/(lM)}{s^2\left[s^2 - g(M+m)/(lM)\right]}, \tag{18}$$

$$G_2(s) = k_v s^3 + \beta s^2 + k_d s + k_p \tag{19}$$

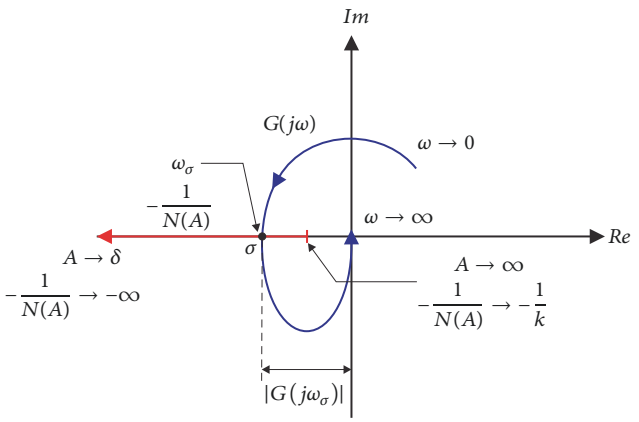

FIGURE 6: Polar plot of $G(j\omega)$ and $-1/N(A)$.

are the plant and controller, respectively, and $g/(lM) > 0$. Furthermore, the magnitude of (17) behaves as a low-pass filter, since $G(s)$ has four poles and only three zeros. Then, a limit cycle may exist if [43], Ch. 5,

$$G(j\omega) = -\frac{1}{N(A)}, \tag{20}$$

which implies that the polar plot of $G(j\omega)$ intersects the negative real axis in the open interval $(-\infty, -1/k)$. This is because $-1/N(A)$ is real and negative. Hence, the oscillation frequency, ω_σ, and the amplitude of the oscillation, A, are found as the values of ω, in $G(j\omega)$, and A, in $-1/N(A)$, at the point σ where their plots intersect [43], Ch. 5. The graphic representation of this is shown in Figure 6.

3.3. Controller Design. The design of the controller gains k_v, β, k_d, and k_p is achieved as described in [20] for the Furuta pendulum case. In this section, particularities of the controller design for the inverted pendulum on a cart case are introduced. Since the following transfer function of the two internal loops is obtained:

$$\frac{-g/(lM)}{s^2 + g/(lM)\, k_v s + [g/(lM)\, \beta - g(M+m)/(lM)]}, \tag{21}$$

when the dead-zone is omitted from Figure 4, then k_v and β must satisfy the following conditions:

$$k_v > 0 \ \wedge \ \frac{g}{lM}\beta > \frac{(M+m)\, g}{lM} \tag{22}$$

to ensure that all coefficients of the characteristic polynomial of the transfer function in (21) are positive.

Now, note that when replacing s by $j\omega$ in (18), the phase of $G_1(j\omega)$ is -360° for all $\omega \geq 0$ because $g/(lM) > 0$ and each one of the factors $1/-\omega^2 < 0$ and $1/(-\omega^2 - g(M+m)/(lM)) < 0$ introduces a phase of -180°. Hence, with the intention of forcing the polar plot of $G(j\omega)$ to intersect the negative real axis, i.e., to render phase of $G(j\omega)$ equal to -180° at some $\omega > 0$, the frequency analysis performed for the controller $G_2(j\omega)$ in [20] is applied. Such an analysis is described below to facilitate the reference.

The phase of $G_2(j\omega)$ must be as follows:

$$\angle G_2(j\omega) = \arctan\left(\frac{k_d\omega - k_v\omega^3}{k_p - \beta\omega^2}\right) = +180^\circ. \tag{23}$$

This implies that the following conditions have to be satisfied:

$$k_d\omega - k_v\omega^3 = 0. \tag{24}$$

$$k_p - \beta\omega^2 < 0. \tag{25}$$

From (24) the following relation to find k_d is obtained:

$$k_d = k_v\omega^2. \tag{26}$$

Lastly, in order to compute k_p, s is replaced by $j\omega$ in controller (19) to obtain the following:

$$\begin{aligned} G_2(j\omega) &= k_v(j\omega)^3 + \beta(j\omega)^2 + k_d(j\omega) + k_p, \\ &= j\left(k_d\omega - k_v\omega^3\right) + \left(k_p - \beta\omega^2\right), \end{aligned} \tag{27}$$

whose magnitude is determined by

$$|G_2(j\omega)| = \sqrt{\left(k_d\omega - k_v\omega^3\right)^2 + \left(k_p - \beta\omega^2\right)^2}. \tag{28}$$

Hence, when solving (28) for k_p, the formula below is obtained:

$$k_p = \pm\sqrt{|G_2(j\omega)|^2 - \left(k_d\omega - k_v\omega^3\right)^2} + \beta\omega^2. \tag{29}$$

Therefore, the sign in this latter expression has to be chosen so that (25) is accomplished.

Finally, to propose the frequency $\omega = \omega_\sigma$ at which it is desired that the polar plot of $G(j\omega)$ intersects the negative real axis it is necessary to compute k_p and k_d. Likewise, the magnitude $|G_2(j\omega_\sigma)|$ that must be introduced by the controller has to be known, for which a desired magnitude of $G(j\omega)$ when $\omega = \omega_\sigma$ has to be proposed. Then, from

$$|G(j\omega_\sigma)| = |G_1(j\omega_\sigma)| \cdot |G_2(j\omega_\sigma)|, \tag{30}$$

the magnitude $|G_2(j\omega_\sigma)|$ can be computed by

$$|G_2(j\omega_\sigma)| = \frac{|G(j\omega_\sigma)|}{|G_1(j\omega_\sigma)|}. \tag{31}$$

Since $|G_1(j\omega_\sigma)|$ can be obtained from the Bode diagrams of $G_1(j\omega)$, then Bode diagrams are a suitable tool to design the controller gains k_v, β, k_d, and k_p.

Until here, the procedure and formulas to compute the controller gains have been described. The procedure to choose such gains in order to eliminate limit cycle due to dead-zone nonlinearity is presented in the next section.

4. Experimental Procedure for Limit Cycle Elimination

In this section, the experimental procedure introduced in [20] is applied to eliminate limit cycles in the inverted

pendulum on a cart. In [20], the procedure to eliminate limit cycle was executed departing from knowing the numerical value δ of the dead-zone nonlinearity of the Furuta pendulum and pendubot. Also, in that paper, it was mentioned that the procedure can be applied without requiring the knowledge of such a parameter. Thus, the procedure in [20] is applied here for the inverted pendulum on a cart without requiring the knowledge of δ. Additional steps that help to better address the procedure, which do not modify the generality of the procedure introduced in [20], are indicated. Also, particularities of the application of the procedure in the inverted pendulum on a cart are indicated in each step.

Before starting the application of the procedure for limit cycle elimination in the inverted pendulum on a cart, the conjecture established in [20] is recalled below.

Conjecture. According to the dead-zone nonlinearity characteristic function depicted in Figure 3, if $|e| \leq \delta$ then a zero value appears at the plant input $c = 0$; i.e., the force applied by the motor to the inverted pendulum on a cart is zero and the mechanism might rest at the operation point defined in (4). Since the threshold δ is uncertain because friction is uncertain, it is natural to wonder whether it is possible to render $A < \delta$ in experiments, despite (13) being only valid for $A \geq \delta$. Recall that $A \geq |e|$ because A is the amplitude of e. Then, the mechanism might rest at the operation point if A is chosen to be small enough; i.e., the limit cycle might vanish under these conditions.

It is also recalled that, according to Figure 6, with the purpose of reducing the amplitude of the limit cycle, the polar plot of $G(j\omega)$ must intersect the negative real axis at a point σ located farther to the left of the point $-1/k = -1$. This latter is computed by considering $k = 1$, which is a value usually set for a conventional DC motor. This suggests that $|G(j\omega_\sigma)| \gg 1$ and this must occur at an oscillation frequency $\omega = \omega_\sigma$.

The procedure to eliminate the limit cycle induced by the dead-zone nonlinearity, when regulating position in the inverted pendulum on a cart, was experimentally applied as follows:

(1) Bode diagrams of the plant $G_1(j\omega)$ were plotted as shown in Figure 7. For this, (18) was used.

(2) The frequency $\omega_\sigma = 6$ rad/s and the magnitude $|G(j\omega_\sigma)| = 22$ were initially proposed. The value of ω_σ was proposed since this renders $f_\sigma = \omega_\sigma/(2\pi) \approx 0.9549$ Hz, which is a reasonable frequency in Hertz for the experimental prototype that was built. Using the value of ω_σ and Bode diagrams plotted in Figure 7, the following magnitude in dB was measured:

$$\left|G_1\left(j\omega_\sigma\right)\right|_{\text{dB}} = -26.1 \text{ dB}, \tag{32}$$

which was converted into

$$\left|G_1\left(j\omega_\sigma\right)\right| = 10^{|G_1(j\omega_\sigma)|_{\text{dB}}/20} = 0.0495. \tag{33}$$

The latter numerical value was used in (31) to compute $|G_2(j\omega_\sigma)|$, finding the following:

$$\left|G_2\left(j\omega_\sigma\right)\right| = \frac{4}{44.1570} = 444.0406. \tag{34}$$

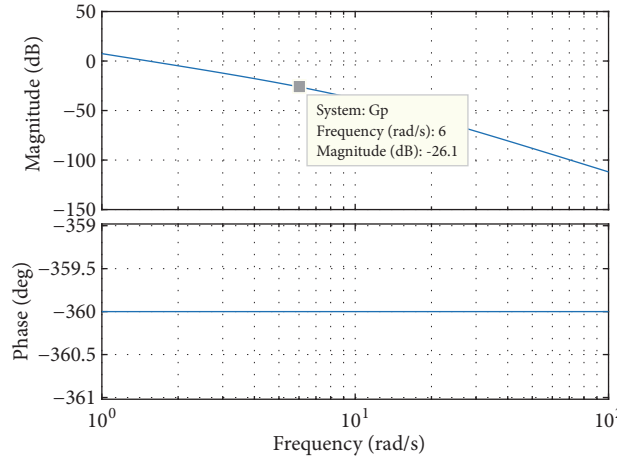

Figure 7: Bode diagrams of $G_1(s)$.

The numerical values of ω_σ and $|G_2(j\omega_\sigma)|$ shall be used to compute k_p.

(3) $k_v = 0.94$ and $\beta = 12.5$ were selected satisfying (22), that is, rendering all coefficients of the characteristic polynomial of (21) positive. Also, the proposed k_v and β achieve that the sign of the square root in (29) is negative, which is implied from (25), and that $k_p > 0$. According to Figure 4, this latter is necessary to ensure closed-loop stability. Note that, in order to avoid negative values for k_p, it is clear from (29) and (25) that larger values of either β or ω_σ are required. From the second degree characteristic polynomial in (21), it is concluded that a larger β is possible if roots of this characteristic polynomial are farther from the origin. This is accomplished since $k_v = 0.94$ and $\beta = 12.5$ assign real poles of (21) at -225.8894 and -13.6275. In the case that the selection of β does not achieve $k_p > 0$ and the designer prefers to increase ω_σ, instead of increasing β, the designer must go back to step (2).

(4) With the numerical values in steps (2) and (3), (29), and (26), k_d and k_p were computed as follows:

$$\begin{aligned} k_d &= 33.84, \\ k_p &= 5.9594. \end{aligned} \tag{35}$$

For (29), a "$-$" sign was chosen because this renders $k_p - \beta\omega_\sigma^2 = -444.0406 < 0$. Notice that this ensures that k_p is real and positive, and hence closed-loop stability is ensured. If this were not the case, the designer would have to go back to step (3).

(5) Through the Bode diagrams of the compensated system $G(s)$ shown in Figure 8, it was corroborated that the open-loop system had the desired phase, -180°, at the desired frequency and magnitude, $\omega_\sigma = 6$ rad/s and $|G(j\omega_\sigma)| = 22 \approx 26.9$ dB, respectively. The corresponding polar plot of $G(j\omega)$ is depicted in Figure 9.

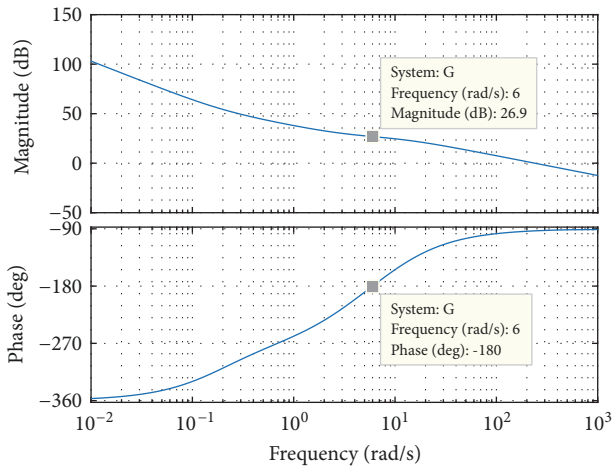

Figure 8: Bode diagrams of $G(s)$.

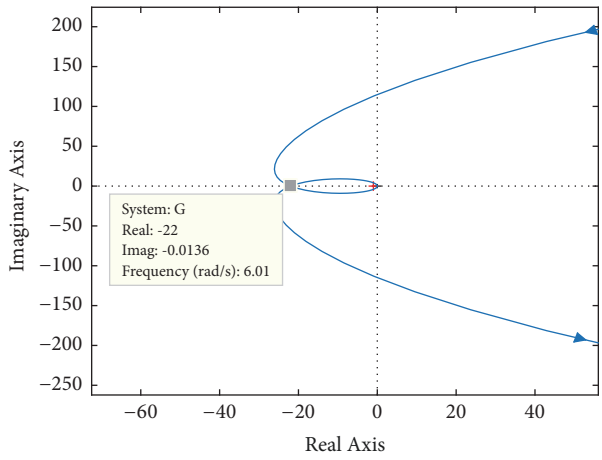

Figure 9: Polar plot of $G(j\omega)$.

(6) Once k_v, β, k_d, and k_p were known, the relations in (16) were used to find the following numerical values for the gains of linear state feedback controller (15):

$$\begin{aligned} k_1 &= -5.9594, \\ k_2 &= -33.84, \\ k_3 &= -123.2209, \\ k_4 &= -12.6054. \end{aligned} \tag{36}$$

Using these gains k_1, k_2, k_3, and k_4, linear state feedback controller (15) was experimentally implemented to regulate the prototype of the inverted pendulum on a cart depicted in Figure 2. Since (15) only stabilizes the prototype at $x_\delta = \mathbf{0}$ when operating close to (4), the pendulum was manually taken to near such an operation point. Hence, the following switching condition was used:

$$f = \begin{cases} (15) & \text{for } \sqrt{\left(\phi - \overline{\phi}\right)^2 + \dot{\phi}^2} \leq 0.3 \\ 0 & \text{for } \sqrt{\left(\phi - \overline{\phi}\right)^2 + \dot{\phi}^2} > 0.3. \end{cases} \tag{37}$$

The experimental results obtained when using (37) with (36) are shown in Figure 10, where a limit cycle is observed. Since there is noise in the control signal f, the amplitude and frequency of the limit cycle are difficult to measure there. But as $e = f(s)$ is linearly related to $F(s)$ through (14), the analysis in Section III about limit cycle is also valid for F. Hence, the amplitude and the frequency of F were measured to observe the behavior of the limit cycle. The measured amplitude of the limit cycle is denoted as A_F and was computed by summing the maximal and the minimum absolute values of F, whereas the measured frequency of the limit cycle is denoted as $\omega_{\sigma F}$ and was computed using the following:

$$\omega_{\sigma F} = \frac{2\pi n}{t_f - t_i}, \tag{38}$$

where n is the number of oscillations that occurred in the time interval between t_i and t_f. Thus, $A_F = 0.4323$ m and $\omega_{\sigma F} = 0.2922$ rad/s were obtained.

(7) As a limit cycle appeared in the previous step, $|G(j\omega_\sigma)|$ was increased and we went back to step (3). When $|G(j\omega_\sigma)| = 38$ was reached, $k_v = 1.66$ and $\beta = 21.5$ were selected. Then, $k_d = 59.7600$ and $k_p = 7.0208$ were computed. Thus, the following gains for controller (15) were computed:

$$\begin{aligned} k_1 &= -7.0208, \\ k_2 &= -59.7600, \\ k_3 &= -211.6171, \\ k_4 &= -22.2606. \end{aligned} \tag{39}$$

When implementing (37) with (39), the results depicted in Figure 11 were obtained. There, it can be observed that the limit cycle was partially eliminated and that $A_F = 0.1371$ m when it appears.

Since in the previous experiment the limit cycle was partially eliminated, $|G(j\omega_\sigma)|$ was incremented so that $|G(j\omega_\sigma)| = 40$. In this case, $k_v = 1.75$ and $\beta = 22.5$ were chosen, $k_d = 63$ and $k_p = 2.6535$ were computed, and the following gains of (15) were found:

$$\begin{aligned} k_1 &= -2.6535, \\ k_2 &= -63, \\ k_3 &= -220.9903, \\ k_4 &= -23.4675. \end{aligned} \tag{40}$$

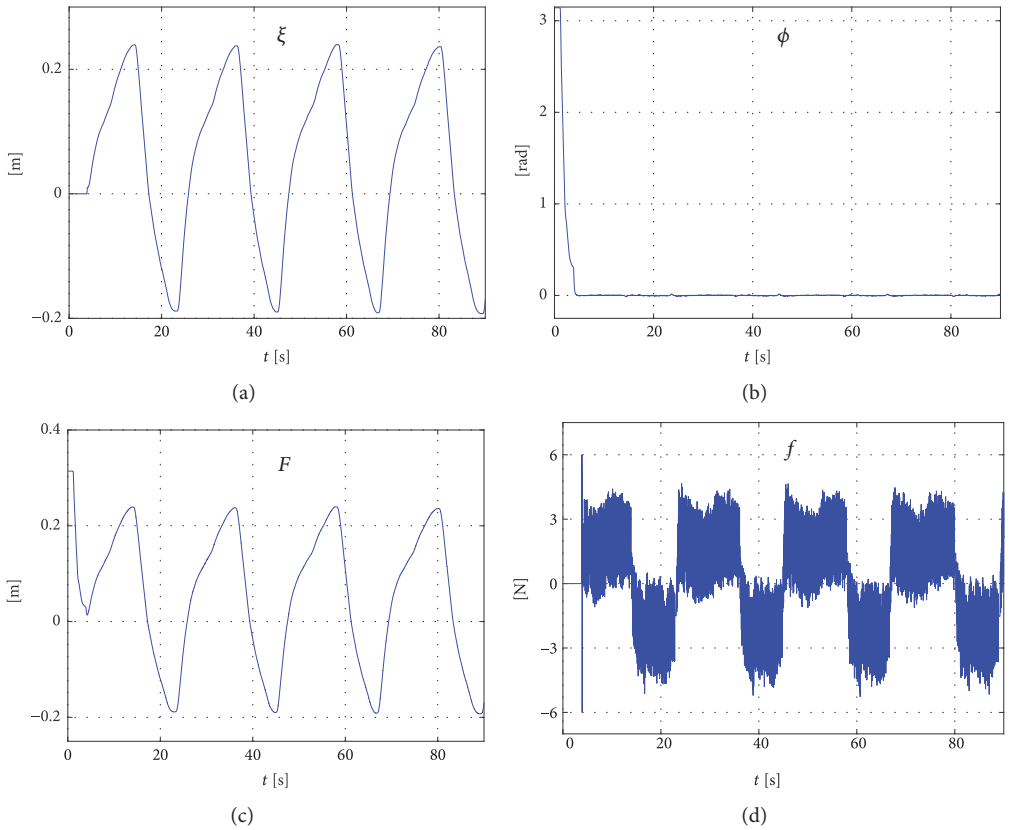

Figure 10: Experimental results when using (36).

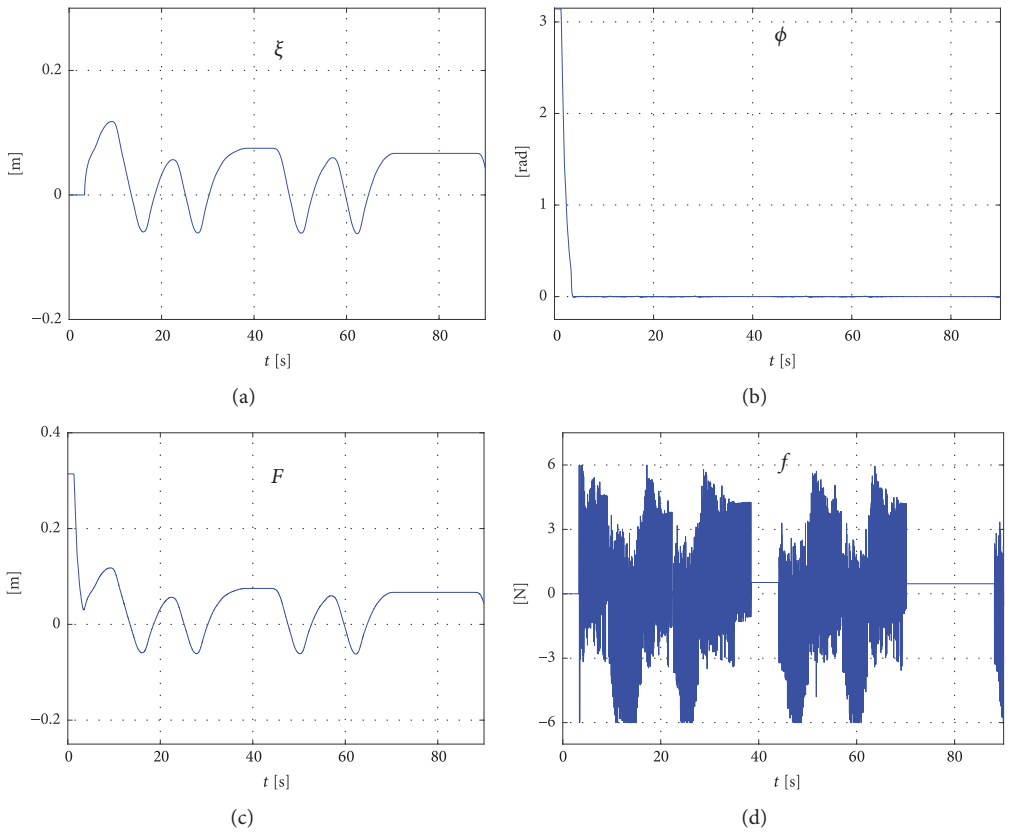

Figure 11: Experimental results when $|G(j\omega_\sigma)| = 38$ and $\omega_\sigma = 6$ rad/s.

Although it may be thought that this time the limit cycle would disappear, after executing the experiment of controller (37) with (40), considerable vibration in the prototype was observed and limit cycle reappeared instead of being eliminated. See experimental results in Figure 12, where $A_F = 0.2901$ m and $\omega_{\sigma F} = 0.2365$ rad/s were measured. It is important to highlight that although limit cycle was not eliminated so far, it was actually reduced since $A_F = 0.2901$ m $< A_F = 0.4323$ m. This is in accordance with the conjecture. Also, note that noise in the control signal f is more noticeable because $|G(j\omega_\sigma)|$ was increased (see Figures 10(d), 11(d), and 12(d)).

(8) Since in the previous step limit cycle was not eliminated and considerable vibration was observed in the prototype (see noise in Figure 12(d)), ω_σ was increased to 8 rad/s, $|G(j\omega_\sigma)| = 22$ was set again, and we went back to step (3). As limit cycle still remains, but with a reduced amplitude of oscillation, $|G(j\omega_\sigma)|$ was increased again. As an example of reduction of limit cycle, with regard to the experimental results in Figure 12, the experimental results when $|G(j\omega_\sigma)| = 34$ are depicted in Figure 13. There, it is remarkable that limit cycle was partially eliminated and little oscillations appeared with $A_F = 0.0786$ m, which is less than the amplitude of limit cycle associated with Figures 11 and 12.

To obtain the results in Figure 13, the following gains of controller (15) were used:

$$\begin{aligned} k_1 &= -4.8351, \\ k_2 &= -97.28, \\ k_3 &= -226.1135, \\ k_4 &= -24.6392. \end{aligned} \tag{41}$$

Such gains were found departing from selecting $k_v = 1.52$ and $\beta = 23$ and computing $k_d = 97.28$ and $k_p = 4.8351$.

(9) Finally, limit cycle disappeared when $|G(j\omega_\sigma)| = 36$ and $\omega_\sigma = 8$ rad/s. For that, $k_v = 1.61$ and $\beta = 24.5$ were chosen, $k_d = 103.04$ and $k_p = 14.5313$ were computed, and the following gains of controller (15) were found:

$$\begin{aligned} k_1 &= -14.5313, \\ k_2 &= -103.04, \\ k_3 &= -241.7981, \\ k_4 &= -26.0981. \end{aligned} \tag{42}$$

The obtained experimental results are shown in Figure 14.

From the experimental results, it was observed that for each ω_σ there is a maximum value of $|G(j\omega_\sigma)|$ allowed by the prototype of the inverted pendulum on a cart to perform experiments. This is because noise in the control signal was increased as $|G(j\omega_\sigma)|$ was increased. The effect of this noise was reflected in the prototype as noticeable vibration when $|G(j\omega_\sigma)|$ reached some high value. Thus, lower frequencies allow larger magnitudes of $G(j\omega)$ and at larger frequencies the magnitude of $G(j\omega)$ must be decreased to avoid noticeable vibration in the closed-loop system and to approach to the limit cycle elimination. Another observation is that the experimental results corroborate the conjecture, i.e., that limit cycle is eliminated as selecting controller gains such that the polar plot of $G(j\omega)$ crosses the negative real axis at a point located farther to the left. Furthermore, an additional observation from the experiments is that limit cycle elimination is accomplished as frequency ω_σ, where the polar plot of $G(j\omega)$ crosses the negative real axis, is chosen larger. Note that these same observations were made for the Furuta pendulum in [20].

On the other hand, some differences were found when comparing frequency $\omega_{\sigma F}$ of the experiments with the desired one. These differences are mainly due to the following:

(i) According to [43], Ch. 5, since the describing function method has an approximate nature, some inaccuracies are found in results: *(a)* the predicted amplitude and frequency might not be accurate, *(b)* a predicted limit cycle might actually not exist, or *(c)* an existing limit cycle is not predicted, the first kind of inaccuracy, i.e., *(a)*, being quite common.

(ii) Dead-zone "transfer function" (13) is an idealization of the nonlinear phenomenon that is actually presented in the practical plant. Hence, not all the dynamics of the dead-zone nonlinearity is concentrated in (13).

Until here it has been shown that the controller and the applied procedure allow elimination of the limit cycle in the inverted pendulum on a cart, but it was previously commented that δ is uncertain because friction is uncertain. This latter implies that knowing the exact value of δ is difficult, which acts as a disturbance. For this reason compensation techniques had to be used to face limit cycle issue online. Thus, it becomes interesting to know the behavior of the linear controller, here implemented for the inverted pendulum on a cart, when the limit cycle in the system changes due to the conditions of operation. Figure 15 presents the results when gains (42) are implemented for the system under study without previously performing an experiment, that is, without "warming up" the actuator. Note that these conditions of operation are different from those when the results of Figure 14 were obtained because then several experiments were consecutively performed before eliminating the limit cycle; that is, the actuator of the system was "warmed up." In Figure 15 it can be observed that in different occasions a limit cycle reappears, which is natural since static friction is greater when there is no previous movement (δ is different). But it is important to remark from Figure 15 is that limit cycle is eliminated after reappearing. Thus, it can be concluded that the simple linear controller here implemented is feasible and robust enough to eliminate limit cycle.

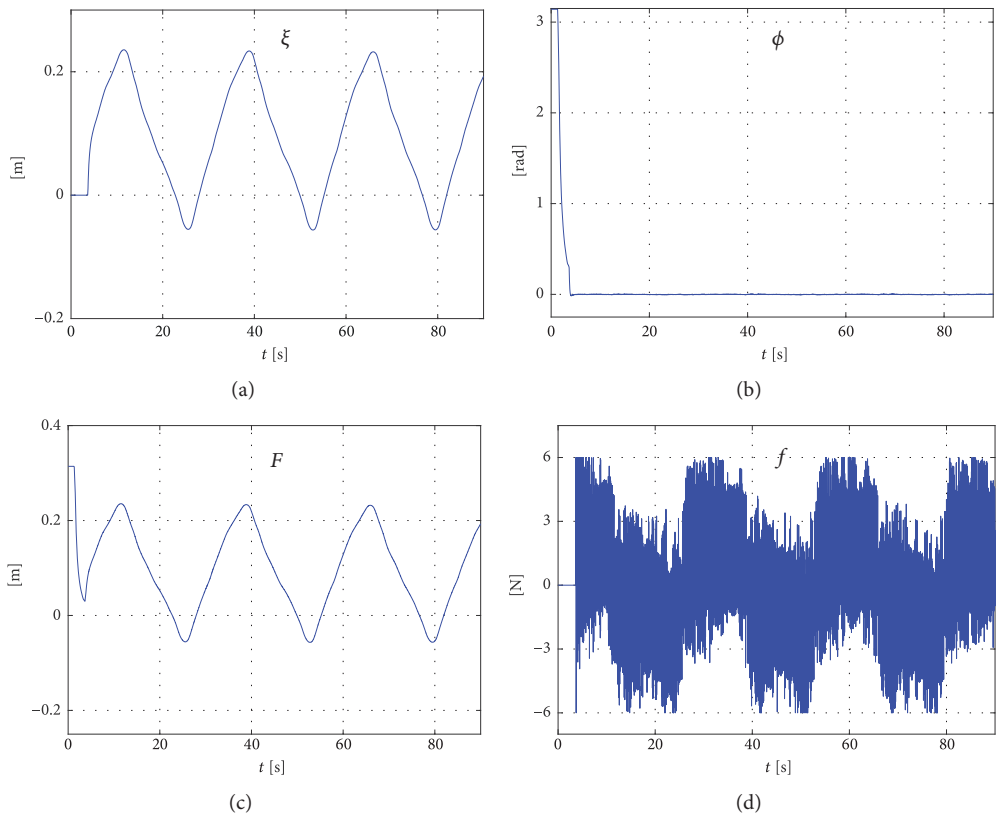

Figure 12: Experimental results when $|G(j\omega_\sigma)| = 40$ and $\omega_\sigma = 6$ rad/s.

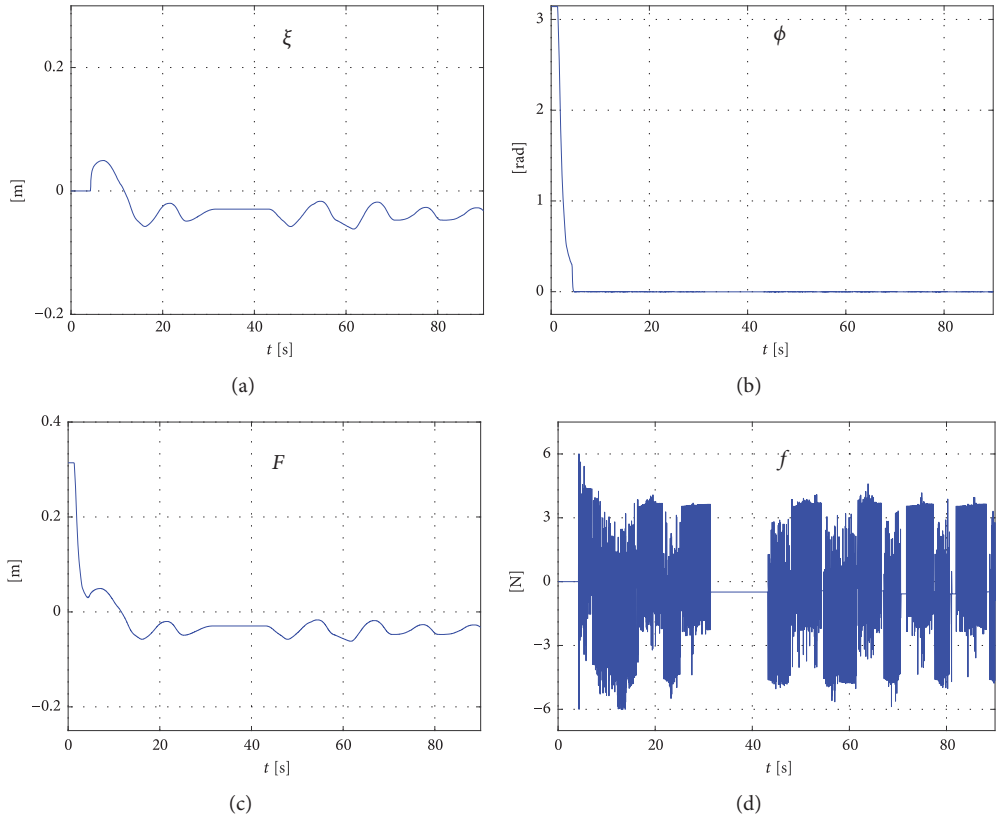

Figure 13: Experimental results when $|G(j\omega_\sigma)| = 34$ and $\omega_\sigma = 8$ rad/s.

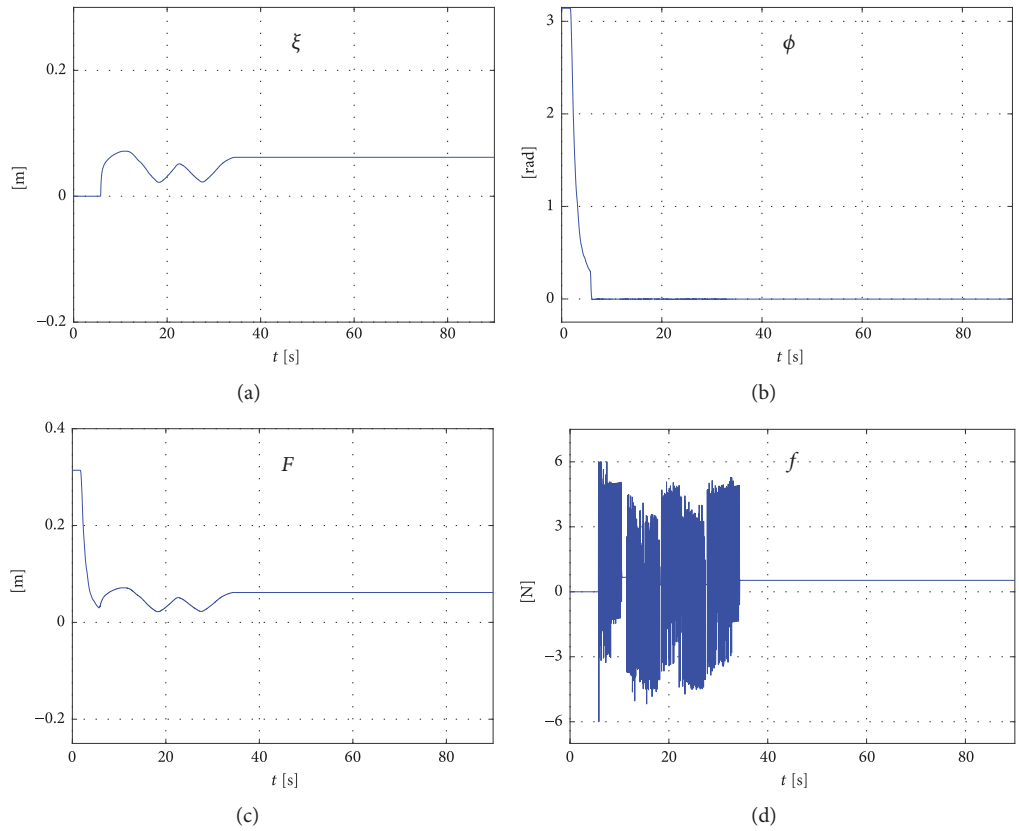

Figure 14: Experimental results when $|G(j\omega_\sigma)| = 36$ and $\omega_\sigma = 8$ rad/s.

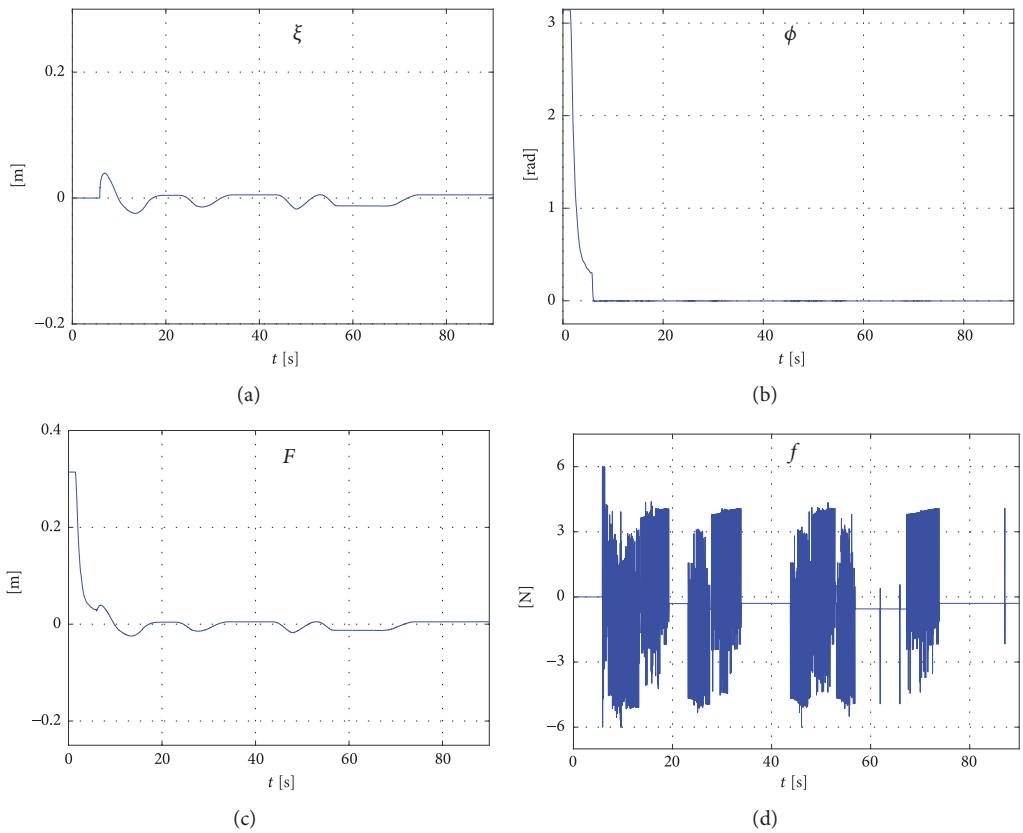

Figure 15: Experimental results when gains (42) are implemented without previously performing an experiment in the prototype.

5. Conclusion

A linear controller based on the frequency response approach and an experimental procedure, introduced recently by the authors for the Furuta pendulum and the pendubot, has been successfully applied to eliminate the limit cycle in the inverted pendulum on a cart. Therefore, from the experimental results, the following can be concluded. *(i)* The inverted pendulum on a cart has similar behavior to that of the Furuta pendulum under the effect of linear state feedback controller (15), when it is designed through frequency response-based controller (14). *(ii)* The applicability of the approach introduced in [20] to eliminate limit cycle is confirmed for another inverted pendulum, corroborating that the approach can eliminate limit cycles in different inverted pendulums. *(iii)* Robustness of the controller is verified when conditions of operation change.

Data Availability

The data used to support the findings of this study are available from the corresponding author upon request.

Conflicts of Interest

The authors declare that the research was conducted in the absence of any commercial, financial, or personal relationships that could be construed as a potential conflict of interest.

Acknowledgments

This work was supported by Secretaría de Investigación y Posgrado del Instituto Politécnico Nacional, México. The work of M. Antonio-Cruz has been supported by the CONACYT-México and BEIFI-IPN scholarships. V. M. Hernández-Guzmán and G. Silva-Ortigoza thank the support given by the SNI-México. Lastly, R. Silva-Ortigoza acknowledges financial support from IPN programs EDI and SIBE and from SNI-México.

References

[1] B. Armstrong-Hélouvry, P. Dupont, and C. C. de Wit, "A survey of models, analysis tools and compensation methods for the control of machines with friction," *Automatica*, vol. 30, no. 7, pp. 1083–1138, 1994.

[2] G. Tao and P. V. Kokotovic, "Adaptive control of plants with unknown dead-zones," *IEEE Transactions on Automatic Control*, vol. 39, no. 1, pp. 59–68, 1994.

[3] G. Tao and F. L. Lewis, *Adaptive Control of Nonsmooth Dynamic Systems*, Springer, New York, NY, USA, 2001.

[4] J. Sandoval, R. Kelly, and V. Santibáñez, "Interconnection and damping assignment passivity-based control of a class of underactuated mechanical systems with dynamic friction," *International Journal of Robust and Nonlinear Control*, vol. 21, no. 7, pp. 738–751, 2011.

[5] A. Nejadfard, M. J. Yazdanpanah, and I. Hassanzadeh, "Friction compensation of double inverted pendulum on a cart using locally linear neuro-fuzzy model," *Neural Computing and Applications*, vol. 22, no. 2, pp. 337–347, 2013.

[6] D. Xia, L. Wang, and T. Chai, "Neural-network-friction compensation-based energy swing-up control of pendubot," *IEEE Transactions on Industrial Electronics*, vol. 61, no. 3, pp. 1411–1423, 2014.

[7] C. Aguilar-Avelar, R. Rodríguez-Calderón, S. Puga-Guzmán, and J. Moreno-Valenzuela, "Effects of nonlinear friction compensation in the inertia wheel pendulum," *Journal of Mechanical Science and Technology*, vol. 31, no. 9, pp. 4425–4433, 2017.

[8] A. Keck, J. Zimmermann, and O. Sawodny, "Friction parameter identification and compensation using the elastoplastic friction model," *Mechatronics*, vol. 47, pp. 168–182, 2017.

[9] H. Olsson and K. J. Åström, "Friction generated limit cycles," *IEEE Transactions on Control Systems Technology*, vol. 9, no. 4, pp. 629–636, 2001.

[10] R. H. Hensen, M. J. van de Molengraft, and M. Steinbuch, "Friction induced hunting limit cycles: a comparison between the LuGre and switch friction model," *Automatica*, vol. 39, no. 12, pp. 2131–2137, 2003.

[11] L. Márton, "On analysis of limit cycles in positioning systems near Striebeck velocities," *Mechatronics*, vol. 18, no. 1, pp. 46–52, 2008.

[12] S.-L. Chen, K. K. Tan, and S. Huang, "Friction modeling and compensation of servomechanical systems with dual-relay feedback approach," *IEEE Transactions on Control Systems Technology*, vol. 17, no. 6, pp. 1295–1305, 2009.

[13] S.-L. Chen, K. K. Tan, and S. Huang, "Limit cycles induced in type-1 linear systems with PID-type of relay feedback," *International Journal of Systems Science*, vol. 40, no. 12, pp. 1229–1239, 2009.

[14] M. M. Z. Shahadat, T. Mizuno, Y. Ishino, and M. Takasaki, "Effect of nonlinearity caused by friction on a negative stiffness control system," *IEEE Transactions on Control Systems Technology*, vol. 22, no. 4, pp. 1385–1395, 2014.

[15] S. Jeon and M. Tomizuka, "Stability of controlled mechanical systems with ideal Coulomb friction," *Journal of Dynamic Systems, Measurement, and Control*, vol. 130, no. 1, pp. 011013-1–011013-9, 2008.

[16] R. Rascón, D. Rosas, and D. Hernandez-Balbuena, "Regulation control of an underactuated mechanical system with discontinuous friction and backlash," *International Journal of Applied Mathematics and Computer Science*, vol. 27, no. 4, pp. 785–797, 2017.

[17] A. Bisoffi, M. Da Lio, A. R. Teel, and L. Zaccarian, "Global asymptotic stability of a PID control system with Coulomb friction," *Institute of Electrical and Electronics Engineers Transactions on Automatic Control*, vol. 63, no. 8, pp. 2654–2661, 2018.

[18] D. J. Block, K. J. Åström, and M. W. Spong, *The Reaction Wheel Pendulum*, M. W. Spong, Ed., Morgan & Claypool, Champaign, IL, USA, 2007.

[19] V. M. Hernandez-Guzman, M. Antonio-Cruz, and R. Silva-Ortigoza, "Linear state feedback regulation of a Furuta pendulum: design based on differential flatness and root locus," *IEEE Access*, vol. 4, pp. 8721–8736, 2016.

[20] M. Antonio-Cruz, V. M. Hernandez-Guzman, and R. Silva-Ortigoza, "Limit cycle elimination in inverted pendulums: Furuta pendulum and pendubot," *IEEE Access*, vol. 6, pp. 30317–30332, 2018.

[21] F. Verduzco, "Control of oscillations from the k-zero bifurcation," *Chaos, Solitons & Fractals*, vol. 33, no. 2, pp. 492–504, 2007.

[22] L. Freidovich, A. Robertsson, A. Shiriaev, and R. Johansson, "Periodic motions of the Pendubot via virtual holonomic constraints: theory and experiments," *Automatica*, vol. 44, no. 3, pp. 785–791, 2008.

[23] L. Freidovich, A. Shiriaev, F. Gordillo, F. Gómez-Estern, and J. Aracil, "Partial-energy-shaping control for orbital stabilization of high-frequency oscillations of the Furuta pendulum," *IEEE Transactions on Control Systems Technology*, vol. 17, no. 4, pp. 853–858, 2009.

[24] S. Andary, A. Chemori, and S. Krut, "Control of the underactuated inertia wheel inverted pendulum for stable limit cycle generation," *Advanced Robotics*, vol. 23, no. 15, pp. 1999–2014, 2009.

[25] L. T. Aguilar, I. M. Boiko, L. M. Fridman, and L. B. Freidovich, "Generating oscillations in inertia wheel pendulum via two-relay controller," *International Journal of Robust and Nonlinear Control*, vol. 22, no. 3, pp. 318–330, 2012.

[26] G. A. Medrano-Cerda, "Robust computer control of an inverted pendulum," *IEEE Control Systems Magazine*, vol. 19, no. 3, pp. 58–67, 1999.

[27] H. Vasudevan, A. M. Dollar, and J. B. Morrell, "Design for control of wheeled inverted pendulum platforms," *Journal of Mechanisms and Robotics*, vol. 7, no. 4, pp. 1–12, 2015.

[28] M. Eom and D. Chwa, "Robust swing-up and balancing control using a nonlinear disturbance observer for the pendubot system with dynamic friction," *IEEE Transactions on Robotics*, vol. 31, no. 2, pp. 331–343, 2015.

[29] G. Pujol and L. Acho, "Stabilization of the Furuta pendulum with backlash using H_∞-LMI technique: experimental validation," *Asian Journal of Control*, vol. 12, no. 4, pp. 460–467, 2010.

[30] A. T. Azar and F. E. Serrano, "Stabilization of mechanical systems with backlash by PI loop shaping," *International Journal of System Dynamics Applications*, vol. 5, no. 3, pp. 21–46, 2016.

[31] J. Moreno-Valenzuela, C. Aguilar-Avelar, S. A. Puga-Guzmán, and V. Santibáñez, "Adaptive neural network control for the trajectory tracking of the Furuta pendulum," *IEEE Transactions on Cybernetics*, vol. 46, no. 12, pp. 3439–3452, 2016.

[32] M. Antonio Cruz, R. Silva Ortigoza, C. Márquez Sánchez, V. M. Hernández Guzmán, J. Sandoval Gutierréz, and J. C. Herrera Lozada, "Parallel computing as a tool for tuning the gains of automatic control laws," *IEEE Latin America Transactions*, vol. 15, no. 6, pp. 1189–1196, 2017.

[33] A. Zhang, X. Lai, M. Wu, and J. She, "Nonlinear stabilizing control for a class of underactuated mechanical systems with multi degree of freedoms," *Nonlinear Dynamics*, vol. 89, no. 3, pp. 2241–2253, 2017.

[34] T. Ortega-Montiel, R. Villafuerte-Segura, C. Vázquez-Aguilera, and L. Freidovich, "Proportional retarded controller to stabilize underactuated systems with measurement delays: Furuta pendulum case study," *Mathematical Problems in Engineering*, vol. 2017, Article ID 2505086, 12 pages, 2017.

[35] X.-S. Wang, C.-Y. Su, and H. Hong, "Robust adaptive control of a class of nonlinear systems with unknown dead-zone," *Automatica*, vol. 40, no. 3, pp. 407–413, 2004.

[36] J. Zhou, C. Wen, and Y. Zhang, "Adaptive output control of nonlinear systems with uncertain dead-zone nonlinearity," *IEEE Transactions on Automatic Control*, vol. 51, no. 3, pp. 504–511, 2006.

[37] S. Ibrir, W. F. Xie, and C.-Y. Su, "Adaptive tracking of nonlinear systems with non-symmetric dead-zone input," *Automatica*, vol. 43, no. 3, pp. 522–530, 2007.

[38] C.-H. Liao, F.-C. Chou, P.-C. Tung, and Y.-D. Chen, "Suppression of limit cycles in servo systems using gain limit compensator," *IEICE Transactions on Fundamentals of Electronics, Communications and Computer Sciences*, vol. E91-A, no. 11, pp. 3293–3296, 2008.

[39] S. Jeon, "Integrator leakage for limit cycle suppression in servo mechanisms with stiction," *Journal of Dynamic Systems, Measurement, and Control*, vol. 134, no. 3, pp. 034502-1–034502-8, 2012.

[40] D. Putra, H. Nijmeijer, and N. van de Wouw, "Analysis of undercompensation and overcompensation of friction in 1DOF mechanical systems," *Automatica*, vol. 43, no. 8, pp. 1387–1394, 2007.

[41] I. Fantoni and R. Lozano, *Non-linear Control for Underactuated Mechanichal Systems*, Springer, London, UK, 2002.

[42] H. Sira-Ramírez and S. K. Agrawal, *Differentially flat systems*, Marcel Dekker Inc., New York, NY, USA, 2004.

[43] J. J. Slotine and W. Li, *Applied nonlinear control*, Prentice-Hall, New Jersey, NJ, USA, 1989.